Optimal architecture for diamond-based wide-field thermal imaging

Rana Tanos, W. Akhtar, Serge Monneret, F. Favaro de Oliveira, G. Seniutinas, M. Munsch, P. Maletinsky, L. Le Gratiet, I. Sagnes, A. Dréau, et al.

Optimal architecture for diamond-based wide-field thermal imaging

Cite as: AIP Advances **10**, 025027 (2020); https://doi.org/10.1063/1.5140030
Submitted: 25 November 2019 . Accepted: 31 January 2020 . Published Online: 18 February 2020

R. Tanos, W. Akhtar, S. Monneret, F. Favaro de Oliveira, G. Seniutinas, M. Munsch, P. Maletinsky, L. le Gratiet, I. Sagnes, A. Dréau, C. Gergely, V. Jacques, G. Baffou, and I. Robert-Philip

Optimal architecture for diamond-based wide-field thermal imaging

Cite as: AIP Advances 10, 025027 (2020); doi: 10.1063/1.5140030
Submitted: 25 November 2019 • Accepted: 31 January 2020 •
Published Online: 18 February 2020

R. Tanos,[1] W. Akhtar,[2] S. Monneret,[3] F. Favaro de Oliveira,[4,5] G. Seniutinas,[4] M. Munsch,[4] P. Maletinsky,[4,5] L. le Gratiet,[6] I. Sagnes,[6] A. Dréau,[1] C. Gergely,[1] V. Jacques,[1] G. Baffou,[3] and I. Robert-Philip[1,a)]

AFFILIATIONS

[1]Laboratoire Charles Coulomb, Université de Montpellier and CNRS, Place Eugène Bataillon, 34095 Montpellier, France
[2]Department of Physics, JMI, Central University, New Delhi 110025, India
[3]Institut Fresnel, CNRS, Aix Marseille University, Centrale Marseille, 13013 Marseille, France
[4]Qnami, Klingelbergstrasse 82, CH-4056 Basel, Swizterland
[5]Department of Physics, University of Basel, Klingelbergstrasse 82, Basel CH-4056, Switzerland
[6]Centre de Nanosciences et de Nanotechnologies, C2N, CNRS - Université Paris-Sud - Université Paris-Saclay, 10 Boulevard Thomas Gobert, 91120 Palaiseau, France

[a)]**Author to whom correspondence should be addressed:** isabelle.philip@umontpellier.fr

ABSTRACT

Nitrogen-vacancy centers in diamonds possess an electronic spin resonance that strongly depends on temperature, which makes them efficient temperature sensors with sensitivity down to a few mK/$\sqrt{\text{Hz}}$. However, the high thermal conductivity of the host diamond may strongly damp any temperature variations, leading to invasive measurements when probing local temperature distributions. In the view of determining possible and optimal configurations for diamond-based wide-field thermal imaging, here, we investigate both experimentally and numerically the effect of the presence of diamonds on microscale temperature distributions. Three geometrical configurations are studied: a bulk diamond substrate, a thin diamond layer bonded on quartz, and diamond nanoparticles dispersed on quartz. We show that the use of bulk diamond substrates for thermal imaging is highly invasive in the sense that it prevents any substantial temperature increase. Conversely, thin diamond layers partly solve this issue and could provide a possible alternative for microscale thermal imaging. Dispersions of diamond nanoparticles throughout the sample appear as the most relevant approach as they do not affect the temperature distribution, although NV centers in nanodiamonds yield lower temperature sensitivities than bulk diamonds.

Thermal imaging, enabling fast and accurate monitoring of heat distribution at sub-micron scales, has become decisive in a broad range of fields from exploratory research up to prototyping and manufacturing in nanomaterials science, nanoelectronics, nanophotonics, or nanochemistry. Various detection schemes are being explored in this respect.[1] These schemes include tip-enhanced infrared or Raman thermometry,[2,3] scanning thermal microscopy (SThM),[4,5] SQUID-based nano-thermometry,[6] or nanoscale fluorescence thermometry, making use of fluorescent nanoparticles either dispersed on the probed sample or attached to the tip of an atomic force microscope (AFM).[7] However, none of these techniques can simultaneously provide fast, sensitive (in the sub-K/$\sqrt{\text{Hz}}$ range), and quantitative thermal imaging with a sub-micron spatial resolution under ambient conditions.

Nitrogen-vacancy (NV) centers in diamonds have garnered growing attention in the last decade, notably because their electron spin resonance can be detected optically[8] and strongly depends on various external perturbations. This dependence has enabled the implementation of highly sensitive NV-based quantum sensors capable of locally probing several physical quantities including strain[9,10] and electric[11,12] and magnetic fields.[13–15] The sensing capabilities of the NV center have also been extended to thermometry,[16] building on the variation of the zero-field splitting parameter of its electron spin sublevels with temperature.[17] A thermal

sensitivity in the range of 100 mK/$\sqrt{\text{Hz}}$ was demonstrated for single NV centers hosted in nanodiamonds[18] and can reach values down to few mK/$\sqrt{\text{Hz}}$ while using NV centers with long spin coherence times embedded in ultrapure bulk diamond samples.[16,18–20] Besides building on the temperature dependence of spin resonance, temperature sensing with NV centers in diamonds can utilize the temperature dependence of their optical response such as the Debye–Waller factor, zero-phonon line, or anti-Stokes photoluminescence wavelength.[21,22] These all-optical schemes have also been extended to other point defects in diamonds, e.g., SiV, GeV, or SnV colored centers.[23–25] Last but not least, the temperature sensitivities of NV centers can be pushed down to few tens of μK/$\sqrt{\text{Hz}}$ by relying on a transduction of temperature gradients on magnetic fields probed by their electronic spins.[26,27]

These thermal sensing modalities can be exploited for thermal imaging. A first strategy consists in grafting a NV-doped nanodiamond at the apex of either an optical fiber or an AFM tip, which is scanned above the surface of the sample to be probed.[28–30] The spatial resolution of thermal imaging is then ultimately limited by the nanodiamond size. Such a *scanning*-NV configuration however requires a complex experimental apparatus and suffers from long acquisition times. In addition, the thermal sensitivity is impaired by the short spin coherence time of NV centers hosted in nanodiamonds. Another approach makes use of *stationary* NV centers in a wide-field detection scheme.[18,19,31] Although the spatial resolution is then fundamentally limited by diffraction (~500 nm), this approach offers faster acquisition times and a simple experimental configuration. To date, wide-field thermal imaging has been solely demonstrated with NV-doped nanodiamonds directly dispersed on the surface of a target sample.

In this paper, we investigate whether this method could be extended to NV centers hosted in an ultrapure bulk diamond sample in view of improving the thermal sensitivity, thanks to the improved NV spin coherence time. To this end, we first experimentally analyze the temperature distribution induced by a micron-sized heat source deposited on the surface of a bulk diamond material. The results are then compared to numerical simulations performed for a bulk diamond, a 100-nm thin diamond membrane deposited on quartz, and nanodiamonds directly dispersed on the heat source. This study shows that any detection scheme based on bulk diamonds is highly perturbative due to the large thermal conductivity of diamonds. Dispersions of nanodiamonds, in the vicinity of a heat source, appear as the most relevant configuration for invasive-less wide-field thermal imaging, while thin diamond membranes could provide an effective option for thermal imaging at microscale.

The heat source here consists of an array of gold nanoparticles illuminated at their plasmonic resonance wavelength.[32,33] We consider 10 × 10 μm^2 assemblies of gold cuboids with the thickness t = 40 nm, width w = 60 nm, and length l ranging from 90 nm to 210 nm. As illustrated in Fig. 1(a), the metallic cuboids are arranged in periodic two-dimensional rectangular patterns, each with constant cuboid dimensions and with a side-to-side distance of 100 nm along the cuboid's width direction and of 1, 6 × l along the cuboid's length direction. These thermoplasmonic arrays were fabricated on two substrates, namely, an ultrapure electronic grade diamond substrate grown by chemical vapor deposition (element 6) and on a quartz substrate used as a reference. The process combines an electron-beam lithography step, the deposition of 5 nm of titanium and 35 nm of gold, followed by a lift-off. Under continuous near-infrared laser illumination at their absorption resonance, the thermoplasmonic structures give rise to a delocalized temperature distribution, fairly uniform throughout the array.[33,34] The increase in temperature induced by the array is then governed, *inter alia*, by the absorption cross-section σ_{abs} of each cuboid, the number N of cuboids forming the array, and the intensity $\mathcal{I}$ of the infrared laser illumination.

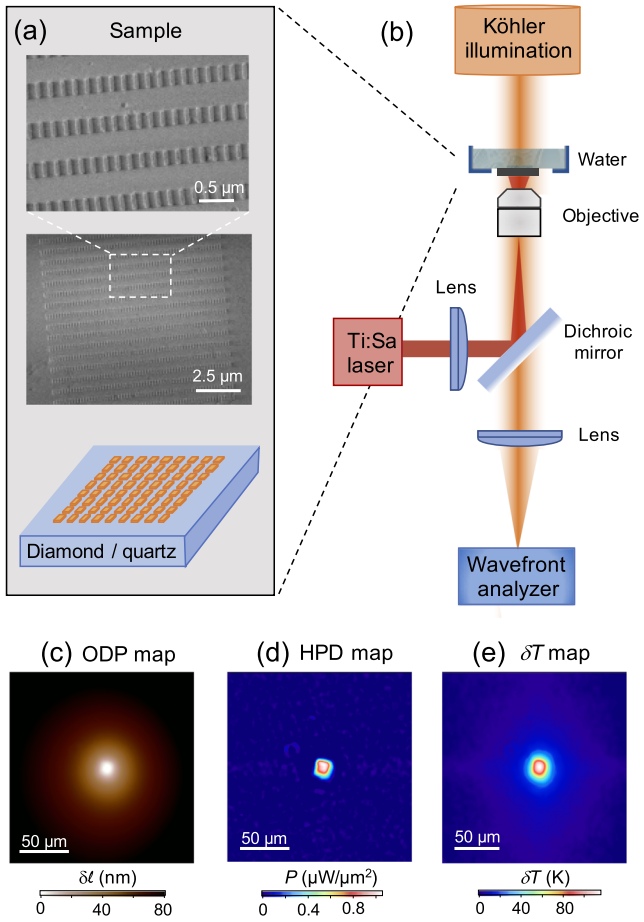

FIG. 1. (a) Scanning electron images of a thermoplasmonic structure deposited on quartz, (b) the schematic of the thermal imaging experimental setup: the thermoplasmonic arrays are surrounded by water and illuminated in a wide-field configuration through a high numerical aperture microscope objective (NA = 0.95) by a tunable infrared Ti:Sapphire laser whose wavelength is set close to the cuboids' plasmonic resonance; a spatially coherent white-light source impinges on the sample on the opposite side, passes through the same objective, and is focused on a wavefront analyzer, which consists of a modified Hartmann grating combined with a CCD camera (Sid4Bio, Phasics SA); the wavefront analyzer records an interferogram on the CCD, which is further processed to retrieve the optical path difference (OPD) generated by the thermal-induced refractive index variations in water, (c) the typical OPD map recorded for a thermoplasmonic array consisting of 60 × 120 nm^2 cross-section cuboids illuminated at 760 nm on the quartz substrate, and [(d) and (e)] resulting maps of heat power density (HPD) and temperature variations.

Temperature variations induced by the thermoplasmonic structures were imaged using quadriwave lateral shearing interferometry[35] [see Fig. 1(b)]. This technique uses a wavefront analyser to indirectly provide temperature distributions with a diffraction-limited spatial resolution and an accuracy of about 1 K. It relies on the temperature-dependent refractive index of a surrounding water layer covering the thermoplasmonic arrays. The heat generated by the arrays results in a steady-state temperature distribution, which provokes modifications in the refractive index in the water. These spatial variations in the refractive index result in a wavefront distortion of a white light source illuminating the sample in a Köhler configuration. Such local distortions are recorded on a wavefront analyser, providing spatially-resolved optical path difference (OPD) maps. A typical OPD map recorded for a thermoplasmonic array deposited on quartz is shown in Fig. 1(c). Post-processing of these data then enables the retrieval of the spatial distribution of the heat power density (HPD) [Fig. 1(d)] and the spatial temperature variations δT [Fig. 1(e)]. This processing relies on a modeling of heat diffusion based on Green's function formalism.[35]

The plasmonic resonance wavelength of the heating structures varies with respect to both the substrate and the shape of the metallic cuboids. In order to obtain a reliable comparison between the heat generated on an ultrapure diamond substrate and on a quartz substrate, experimental conditions leading to similar absorption cross-sections of the thermoplasmonic arrays were carefully selected. As explained in detail in Ref. 35, the absorbed power P_{abs} can be inferred through a spatial integration of the HPD image. The absorption cross-section is then given by $\sigma_{abs} = P_{abs}/(\mathcal{I} \times N)$, where $\mathcal{I}$ is the infrared laser intensity (power per unit area), and N is the number of cuboids forming the thermoplasmonic array. Similar absorption cross-sections, $\sigma_{abs} \sim 2 \times 10^4$ nm^2, were found for (i) 60 × 120 nm^2 cross-section cuboids illuminated at 760 nm on the quartz substrate and (ii) 60 × 90 nm^2 cross-section cuboids illuminated at 710 nm on the diamond substrate.

Under such experimental conditions, thermal images were recorded while increasing the absorbed infrared laser power P_{abs}. As shown in Fig. 2, the maximum local heating δT_{max} evolves linearly with P_{abs} for both substrates, as expected. However, for equivalent absorption powers, the heating induced by the thermoplasmonic array on the quartz substrate is much higher than the one observed on the diamond substrate. A difference of two orders of magnitude is observed, with a maximum heating per absorbed power of 38 K/mW and 0.2 K/mW for quartz and diamond substrates, respectively. This discrepancy results from the large difference in thermal conductivity κ of the substrates. While κ is about 1.4 W/(m K) in quartz, it reaches values almost three orders of magnitude higher in diamonds, with κ = 1000–3300 W/(m K) depending on its purity. Consequently, while heat dissipation in a quartz material is rather low, heat transfer in diamonds is highly efficient. As such, the diamond substrate acts as a thermal sink that cools the heat source.[36] Any architecture of thermal imagers based on bulk diamonds will thus be perturbative: the measured temperature, though recorded with a high sensitivity, will be the temperature of the heat source however significantly cooled by the diamond substrate hosting the NV centers probes and down to temperatures that may be too small to be measured. This precludes the use of bulk diamond samples for wide-field thermal imaging.

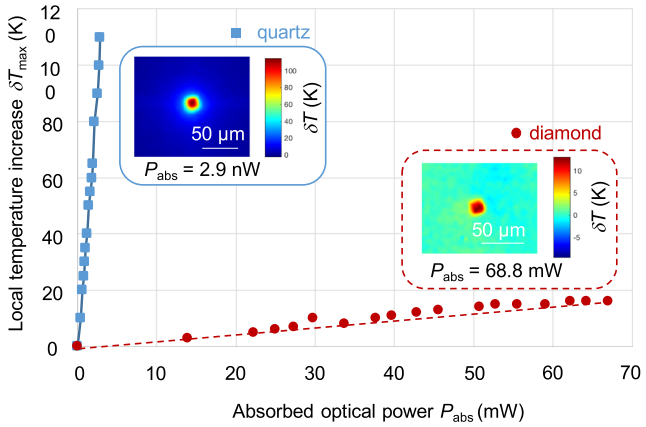

FIG. 2. Maximum local heating δT_{max} as a function of the absorbed optical power P_{abs} for thermoplasmonic arrays deposited on quartz (blue squares) and diamonds (red dots); insets: temperature maps recorded (i) on the quartz substrate for P_{abs} = 2.9 mW leading to δT_{max} = 115.2 °C (top within the blue frame) and (ii) on the diamond substrate for an absorbed laser power of P_{abs} = 68.8 mW leading to δT_{max} = 12.8 °C (bottom within the red frame); solid lines are linear fits of the experimental data.

In order to reduce heat dissipation in bulk diamonds, one alternative approach could be to rely on a thin diamond membrane bonded on a low thermal conductivity substrate, such as quartz. Figure 3 gathers finite-difference time-domain (FDTD) simulations based on heat conduction modeling of temperature increase as a function of heat power for three different diamond-based

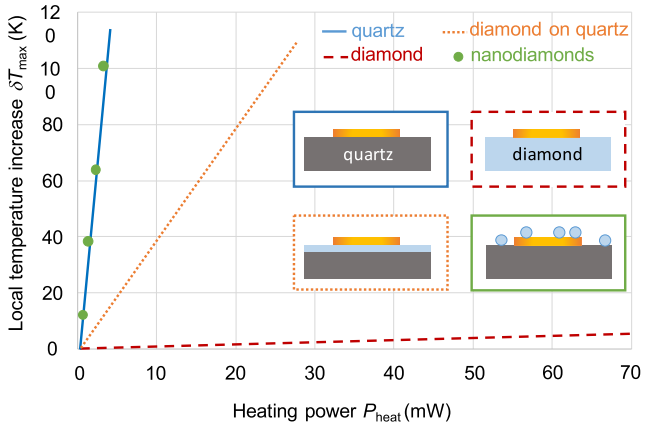

FIG. 3. Numerical simulations of the maximum local heating δT_{max} at the sample surface induced by a two-dimensional 10 × 10 μm^2 heater for increasing heat powers P_{heat}; four configurations are considered: the hot plate located either on a diamond substrate (red dash line), on a quartz substrate (blue solid line), on a 100-nm thick diamond membrane bonded on a quartz substrate (orange dotted line), or on a quartz substrate with diamond nanostructures dispersed on the surface (green dots); in this latter architecture, temperature increase is the one reached within the nanostructures whose dimensions are in the range of few tens of nanometers; the insets show schematics of the four configurations; the temperature increase per heating power reaches ≃4 K/mW in the heterostructure geometry; it is almost two orders of magnitude higher than the one predicted on bulk diamonds and is solely ≃6 or 7 times smaller than the one expected on the quartz geometry.

architectures: (i) a bulk diamond, (ii) a 100-nm thin diamond membrane on quartz, and (iii) nanodiamonds dispersed on the heat source. The achieved temperature increase in the diamond–quartz heterostructure is much higher than the one predicted for bulk diamonds and gets closer to the one expected on quartz. This stems from the strongly reduced effective thermal conductivity of the diamond–quartz heterostructure, in which the effective heat release through diamonds occurs no longer in three but in two dimensions. In view of applications for thermal imaging, this partly lifts the limitations encountered with bulk diamonds. However, the heat diffusion throughout the diamond layer would still yield a lateral spreading of temperature distribution over a length scale of a few μms, thus limiting the spatial resolution.

Conversely, the temperature of nanodiamonds exactly matches the one expected on the low thermal conductivity quartz substrate (see Fig. 3), with a homogenous temperature distribution across the entire nanodiamond volume. This thermalization of the nanodiamonds with the local thermal bath, combined with the constant temperature profile within the nanoparticle, allows for a non-perturbative measurement of the heat source temperature, despite the randomness in the position of the NV spin sensor inside the nanodiamond.

These results enable us to specify the optimal configuration for NV-based wide-field thermal imaging. Although bulk diamond imagers would provide the highest temperature sensitivity due to increased spin coherence times, efficient heat transfer in such high thermal conductivity material unavoidably leads to significant cooling of the sample to be probed, thus preventing any effective temperature mapping at sub-micron scales. Engineered heterostructures stacking thin diamond membranes over low conductive substrates feature significantly reduced heat diffusion, providing a valuable option for imaging at microscale. The most relevant configuration for non-invasive wide-field thermal imaging yet consists of random or ordered dispersions of diamond nanostructures on the hot sample to be probed. These thermal imagers may bring competitive imaging modalities with implications in the fields of micro- and nano-electronics, nanoplasmonics, or chemistry at nanoscale.

The authors acknowledge financial support from the French Research National Agency (through the ANR THESEUS Grant), the Center National de la Recherche Scientifique (through the CNRS TEMPO Grant), and the European Commission (through H2020 program's ASTERIQS, TSAR, and ThermoQuant grants). This work was also partly supported by the French RENATECH network.

REFERENCES

[1] M. Quintanilla and L. M. Liz-Marzand, "Guiding rules for selecting a nanothermometer," Nano Today **19**, 126 (2018).
[2] Q. Weng, S. Komiyama, L. Yang, Z. An, P. Chen, S.-A. Biehs, Y. Kajihara, and W. Lu, "Imaging of nonlocal hot-electron energy dissipation via shot noise," Science **360**, 775 (2018).
[3] L. Li, K. Liu, B. Suen, Q. Liu, F. E. King, and A. Talke, "Numerical and experimental study of near-field heating using tip-enhanced Raman spectroscopy (TERS)," Tribol. Lett. **66**, 26 (2018).
[4] A. Majundar, "Scanning thermal microscopy," Annu. Rev. Mater. Sci. **29**, 505–585 (1999).
[5] S. Gomes, A. Assy, and P.-O. Chapuis, "Scanning thermal microscopy: A review," Phys. Status Solidi A **212**, 477–494 (2015).
[6] D. Halbertal, J. Cuppens, M. Ben Shalom, L. Embon, N. Shadmi, Y. Anahory, H. R. Naren, J. Sarkar, A. Uri, Y. Ronen, Y. Myasoedov, L. S. Levitov, E. Joselevich, A. K. Geim, and E. Zeldovn, "Nanoscale thermal imaging of dissipation in quantum systems," Nature **539**, 407–410 (2016).
[7] L. Aigouy, G. Tessier, M. Mortier, and B. Charlot, "Scanning thermal imaging of microelectronic circuits with a fluorescent nanoprobe," Appl. Phys. Lett. **87**, 184105 (2005).
[8] A. Gruber, A. Dräbenstedt, C. Tietz, L. Fleury, J. Wrachtrup, and C. V. Borczyskowski, "Scanning confocal optical microscopy and magnetic resonance on single defect centers," Science **276**, 2012–2014 (1997).
[9] M. E. Trusheim and D. Englund, "Wide-field strain imaging with preferentially aligned nitrogen-vacancy centers in polycrystalline diamond," New J. Phys. **18**, 123023 (2016).
[10] D. A. Broadway, B. C. Johnson, M. S. J. Barson, S. E. Lillie, N. Dontschuk, D. J. McCloskey, A. Tsai, T. Teraji, D. A. Simpson, A. Stacey, J. C. McCallum, J. E. Bradby, M. W. Doherty, L. C. L. Hollenberg, and J.-P. Tetienne, "Microscopic imaging of the stress tensor in diamond using *in situ* quantum sensors," Nano Lett. **19**, 4543–4550 (2019).
[11] F. Dolde, H. Fedder, M. W. Doherty, T. Nöbauer, F. Rempp, G. Balasubramanian, T. Wolf, F. Reinhard, L. C. L. Hollenberg, F. Jelezko, and J. Wrachtrup, "Electric-field sensing using single diamond spins," Nat. Phys. **7**, 459–463 (2011).
[12] J. Michl, J. Steiner, A. Denisenko, A. Bulau, A. Zimmermann, K. Nakamura, H. Sumiya, S. Onoda, P. Neumann, J. Isoya, and J. Wrachtrup, "Robust and accurate electric field sensing with solid state spin ensembles," Nano Lett. **19**, 4904–4910 (2019).
[13] C. L. Degen, F. Reinhard, and P. Cappellaro, "Quantum sensing," Rev. Mod. Phys. **89**, 035002 (2017).
[14] L. Rondin, J.-P. Tetienne, T. Hingant, J.-F. Roch, P. Maletinsky, and V. Jacques, "Magnetometry with nitrogen-vacancy defects in diamond," Rep. Prog. Phys. **77**, 056503 (2014).
[15] E. V. Levine, M. J. Turner, P. Kehayias, C. A. Hart, N. Langellier, R. Trubko, D. R. Glenn, R. R. Fu, and R. L. Walsworth, "Principles and techniques of the quantum diamond microscope," Nanophotonics **8**, 1945 (2019).
[16] G. Kucsko, P. C. Maurer, N. Y. Yao, M. Kubo, H. J. Noh, P. K. Lo, H. Park, and M. D. Lukin, "Nanometre-scale thermometry in a living cell," Nature **500**, 54 (2013).
[17] V. M. Acosta, E. Bauch, M. P. Ledbetter, A. Waxman, L.-S. Bouchard, and D. Budker, "Temperature dependence of the nitrogen-vacancy magnetic resonance in diamond," Phys. Rev. Lett. **104**, 070801 (2010).
[18] P. Neumann, I. Jakobi, F. Dolde, C. Burk, R. Reuter, G. Waldherr, J. Honert, T. Wolf, A. Brunner, J. H. Shim, D. Suter, H. Sumiya, J. Isoya, and J. Wrachtrup, "High-precision nanoscale temperature sensing using single defects in diamond," Nano Lett. **13**, 2738–2742 (2013).
[19] J. Wang, F. Feng, J. Zhang, J. Chen, Z. Zheng, L. Guo, W. Zhang, X. Song, G. Guo, L. Fan, C. Zou, L. Lou, W. Zhu, and G. Wang, "High-sensitivity temperature sensing using an implanted single nitrogen-vacancy center array in diamond," Phys. Rev. B **91**, 155404 (2015).
[20] D. M. Toyli, C. F. de las Casas, D. J. Christle, V. V. Dobrovitski, and D. D. Awschalom, "Fluorescence thermometry enhanced by the quantum coherence of single spins in diamond," Proc. Natl. Acad. Sci. U. S. A. **110**, 8417–8421 (2013).
[21] T. T. Tran, B. Regan, E. A. Ekimov, Z. Mu, Y. Zhou, W. Gao, P. Narang, A. S. Solntsev, M. Toth, I. Aharonovich, and C. Bradac, "Anti-Stokes excitation of solid-state quantum emitters for nanoscale thermometry," Sci. Adv. **5**, eaav9180 (2019).
[22] T. Plakhotnik, M. W. Doherty, J. H. Cole, R. Chapman, and N. B. Manson, "All-optical thermometry and thermal properties of the optically detected spin resonances of the NV-center in nanodiamond," Nano Lett. **14**, 4989 (2014).
[23] C. T. Nguyen, R. E. Evans, A. Sipahigil, M. K. Bhaskar, D. D. Sukachev, V. N. Agafonov, V. A. Davydov, L. F. Kulikova, F. Jelezko, and M. D. Lukin, "All-optical nanoscale thermometry with silicon-vacancy centers in diamond," Appl. Phys. Lett. **112**, 203102 (2018).
[24] J.-W. Fan, I. Cojocaru, J. Becker, I. V. Fedotov, M. H. A. Alkahtani, A. Alajlan, S. Blakley, M. Rezaee, A. Lyamkina, Y. N. Palyanov, Y. M. Borzdov, Y.-P. Yang, A. Zheltikov, P. Hemmer, and A. V. Akimov, "Germanium-vacancy color center in diamond as a temperature sensor," ACS Photonics **5**, 765 (2018).

[25]M. Alkahtani, I. Cojocaru, X. Liu, T. Herzig, J. Meijer, J. Kupper, T. Luhmann, A. V. Akimov, and P. R. Hemmer, "Tin-vacancy in diamonds for luminescent thermometry," Appl. Phys. Lett. **112**, 241902 (2018).
[26]N. Wang, G.-Q. Liu, W.-H. Leong, H. Zeng, X. Feng, S.-H. Li, F. Dolde, H. Fedder, J. Wrachtrup, X.-D. Cui, S. Yang, Q. Li, and R.-B. Liu, "Magnetic criticality enhanced hybrid nanodiamond thermometer under ambient conditions," Phys. Rev. X **8**, 011042 (2018).
[27]C.-F. Liu, W.-H. Leong, K. Xia, X. Feng, A. Finkler, A. Denisenko, J. Wrachtrup, A. Li, and R.-B. Liu, "Ultra-sensitive hybrid diamond nanothermometer," arXiv:1912.12097 [quant-ph] (2019).
[28]I. V. Fedotov, S. Blakley, E. E. Serebryannikov, N. A. Safronov, V. L. Velichansky, M. O. Scully, and A. M. Zheltikov, "Fiber-based thermometry using optically detected magnetic resonance," Appl. Phys. Lett. **105**, 261109 (2014).
[29]A. Laraoui, H. Aycock-Rizzo, Y. Gao, X. Lu, E. Riedo, and C. A. Meriles, "Imaging thermal conductivity with nanoscale resolution using a scanning spin probe," Nat. Commun. **6**, 8954 (2015).
[30]J.-P. Tetienne, A. Lombard, D. A. Simpson, C. Ritchie, J. Lu, P. Mulvaney, and L. C. L. Hollenberg, "Scanning nanospin ensemble microscope for nanoscale magnetic and thermal imaging," Nano Lett. **16**, 326–333 (2016).
[31]P. Andrich, J. Li, X. Liu, F. J. Heremans, P. F. Nealey, and D. D. Awschalom, "Microscale-resolution thermal mapping using a flexible platform of patterned quantum sensors," Nano Lett. **18**, 4684–4690 (2018).
[32]G. Baffou and R. Quidant, "Thermo-plasmonics: Using metallic nanostructures as nano-sources of heat," Laser Photonics Rev. **7**, 171–187 (2013).
[33]G. Baffou, P. Berto, E. Bermudez Urena, R. Quidant, S. Monneret, J. Polleux, and H. Rigneault, "Photoinduced heating of nanoparticle arrays," ACS Nano **7**, 6478–6488 (2013).
[34]H. H. Richardson, M. T. Carlson, P. J. Tandler, P. Hernandez, and A. O. Govorov, "Experimental and theoretical studies of light-to-heat conversion and collective heating effects in metal nanoparticle solutions," Nano Lett. **9**, 1139–1146 (2009).
[35]G. Baffou, P. Bon, J. Savatier, J. Polleux, M. Zhu, M. Merlin, H. Rigneault, and S. Monneret, "Thermal imaging of nanostructures by quantitative optical phase analysis," ACS Nano **6**, 2452–2458 (2012).
[36]K. Setoura, Y. Okada, D. Werner, and S. Hashimoto, "Observation of nanoscale cooling effects by substrates and the surrounding media for single gold nanoparticles under cw-laser illumination," ACS Nano **7**, 7874–7885 (2013).